Vol. 42, No. 3 (2020) 382-399, DOI: 10.24874/ti.803.11.19.06

Tribology in Industry

www.tribology.rs

RESEARCH

Computational Investigation of Erosion Wear on Industrial Centrifugal Pump Handling Solid-Water Flows

J. Kumar[a], G. Tiwari[a], A. Rawat[a,*], V.K. Patel[a]

[a] *Department of Applied Mechanics, MNNIT Allahabad, Prayagraj, 211004, Uttar Pradesh, India.*

Keywords:

Erosion
Solid-water flows
Industrial Pumps
CFD
Stainless steel

* Corresponding author:

Anubhav Rawat
E-mail: Anubhav-r@mnnit.ac.in
Anubhav_1982@yahoo.com

Received: 29 November 2019
Revised: 5 April 2020
Accepted: 1 June 2020

A B S T R A C T

The Centrifugal pumps handling solid-water mixture are heavily afflicted by erosion occurring due to the transportation of solid particles. Eventually, the erosion leads to degradation in performance and mechanical properties of the pump materials. The objective of present work is twofold; a comprehensive erosion study on three of the common pump materials (Carbon Steel, SS 304 and SS 316) by considering solid-water mixture with two different erodent materials (Silicon Carbide and Silicon dioxide), and to find the critical locations of erosion wear on the pump by utilizing commercial CFD code ANSYS R16.0 Fluent. Numerical simulations on a 3-D model of the pump have been conducted and the erosion rates caused due to erodent (SiC and SiO_2) in various parts of the pump namely spiral casing, front Shroud, back shroud and vanes have been calculated for pump materials carbon steel, SS 316 and SS 304 with the concentrations of erodent varying from 5-25 % and at fixed speed of 1450 rpm. Erosion on carbon steel is found to be 1.15-4.16 times higher than the other two steel for all parts at 25 % concentration for SiC erodent material. The corresponding figure for SiO_2 is 1.25-2. Further, it is observed that Casing receives 7-13 times higher erosion than Shrouds and 4-7 times higher than vanes for SiC. Whereas, the wear due to SiO_2 is found to be around 12-30 times higher than SiC at 25 % concentration. Thus, Carbon steel receives more wear and SiO_2 causes more wear over the pump parts. Erosion is not only found to be critically dependent upon pump and erodent materials but also on the interaction of the erodent material with pump material surface. In general, Erosion is found to be increasing linearly with concentration and causing unequal wear at each part of the pump. It is also found that the critical parts for erosion wear of the industrial pumps are where flow suddenly changes direction.

1. INTRODUCTION

Transportation of solid-liquid mixtures through pipelines is a vastly used method in many industries. Few industries do it on purpose to handle solid- liquid flows viz. Transportation of minerals and coal ash through pipelines. Many industries design their pump systems to transport single-phase liquids only but the dispersed phase manifests itself as an impurity. Hydraulic power plants are one such example, where the pumps are designed to handle water flows only. Still, the presence of sand solid particles not only changes the flow characteristics across them but also cause a substantial amount of erosion wear to them. This will deplete the wall thickness of pump at various locations and ultimately may cause failure of pumps many years before their designed life. The failure of operational pumps is severely associated with heavy losses in terms of money incurred both in maintenance or replacement of the pumps and delays in operations at hydraulic power plants. Mainly, two mechanisms by which solid-liquid flow causes material depletion to the pumps are cavitation and slurry erosion due to the solid particles present in the liquid flow. The type of solid-liquid mixture (slurry) determines the characteristics of solid particles present, such as their diameter and concentration.

A peculiar and prevalent problem in the soda ash-making industry is the erosion caused by lime slurry, and complications are compounded due to properties of the surface, erodent, and slurry involved. Extensive experimental and numerical analysis have been carried out over the years in the field of pump and pump casing erosion, specifically into the erosion of surfaces Kishore et al. [1] studied the effect of thermo mechanical processing of steels on the sand slurry erosion behavior using a pot tester. They studied slurry erosion resistance of 13Cr4Ni stainless steel after thermo-mechanical processing and predicted that the thermo-mechanically processed specimens show higher slurry erosion resistance as compared to the as-received stainless steel. Gupta et al. [2] studied sand-water slurry erosion behavior on white cast iron under crayon conditions. More et al. [3] studied the erosion wear characteristics of SS304 using Taguchi technique using a pot tester. They did a detailed parametric study considering the effect of particle size, velocity and concentration. Aribo et al. [4] did a comprehensive erosion-corrosion combined study in a pot tester due to slurry. Adnan et al. [5] predicted that the erosion damage in lime slurry pumps obtained using three-dimensional numerical analysis is directly correlated to impact velocity, concentration by weight and diameter of solid particles along with the critical role played by temperature. It is also reported that the tongue and belly of spiral casing are highly erosive. Rahul et al. [6] found out the ways to estimate the pump efficiency and the erosion of centrifugal pumps used for hydraulic transportation of solids based on optimization of pump design, selection of pump material, concentration and flow characteristics of slurry and ways to optimize both performance and erosion and further used Eulerian-Eulerian model to predict the effect of solids on the performance of centrifugal pumps and the head and efficiency show a decline with the increase in the particle size and concentration. Whereas, high specific gravity particles mitigate the effect of a decrease in head and efficiency of pumps to an extent.

Gautam et al. [7] studied the slurry erosive behavior of brass with sand particle slurry, and according to them, the rate of material loss was found to be dependent on r concentration of sand and also impact velocity. They also predicted that the wear rate aggravates with impingement angles up to 60^0 and declines thereafter. W.K. Chan [8] based on their experimental work on a centrifugal impeller in a closed circuit found that erosion rate increases below the critical NPSH (net positive suction head), then decreases and ultimately increases for a declining NPSH. Gandhi et al. [9] have studied erosion wear for the parallel flow of solid-liquid mixture flows in a slurry pot tester and have found an increase in parallel flow wear with the increase in solid concentration, particle size, and velocity. However, dependency on velocity is greater compared to concentration. Contrary to this, Rawat et al. [10] found the dependency of erosion wear on concentration to be more pronounced than velocity at high concentrations. Yuan et al. [11] employed Bitter's model to ascertain wear coefficients associated with erosion by particle impingement. Pagolthivarthi et al. [12] carried out a predictive analysis of the slurry flow in

centrifugal pump casings with respect to conditions pertaining to geometry and other working conditions. They found that a gradient exists with respect to the solid wall shear and Solid concentration with a gradual increase from the upstream tongue to the downstream belly region. Kaushal et al. [13] estimated pressure drop, concentration profile at various flow conditions, and solid concentration inside a horizontal pipeline. Mesa et al. [14] reported that slurry of an acidic solution consisting of hard particles causes extensive loss in the material on interaction with commercial stainless steel 410 and AISI 420. Satish [15] carried out a study to understand the erosion wear phenomenon in the pump at varied speed settings with different particle size distribution and concentration with the help of ANSYS-CFX computational fluid dynamics software. Xiao et al. [16] used a stainless-steel prototype to study the change in the flow characteristics and erosion mechanism due to material loss and subsequent geometry distortion. Two models were used for the study of the matter in the Eulerian frame of reference, and the results indicated a great reliance on flow characteristics and erosion patterns on geometric variations. Kumar et al. [17] studied the erosion behavior of AISI 316 pipe bend with the implication of a swirl of different vane angles, and Baghel et al. [18] studied the erosion wear on hot forged materials.

Few more important wear related [19-21] studies are worth mentioning but as far as erosion wear studies on pumps are concerned many useful studies [22-32] are previously done on various experimental and numerical aspects related to erosion wear on pumps but in general for a single material and there is no detailed comparative study on special pump materials namely Carbon Steel, SS304 and SS316 that too considering the flow of solid-liquid mixture with the erodent materials of Silicon Carbide (SiC) and Silicon dioxide (SiO_2) as far as centrifugal pumps handling sands in hydraulic power plants is concerned. The study is also essential, and rare in terms of observing the patterns of erosion wear at different locations and parts of the pump viz. casing, vanes, shrouds etc. Real-time experimentations are costly, and there is no established numerical strategy in pump design for wear considering the above mentioned scope. Numerical simulation using CFD facilitates this visualization and critical analysis of three-dimensional complex flows in the pumps and also aids in its hydraulic design. Thus, simulation results are employed in the performance determination of the pump and to alter or eliminate the experiments required in the pump design process. In particular, this becomes important for pumps in hydraulic power plants dealing with sand as an impurity. A 3-D model of a centrifugal pump provided by Kirloskar Pvt. Ltd. is used in the present work to investigate the rate of erosion at the pump casing, impeller blades, and hub. The rate of erosion depends on various parameters like velocity, angle of impact of the solid particle, particle diameter, concentration of the erodent particles, type of erodent particle etc. Different materials respond differently to a change in these parameters. The present work, therefore, aims to investigate the rate of erosion at various components of the pump for commonly used pump materials such as carbon steel, stainless steel 304, and stainless steel 316 at a designed speed of 1450 rpm. A comparison of erosion rates at different components of the pump is imperative for the aforementioned pump materials to determine the suitability of these materials from an erosion resistance standpoint. The change in erosion owing to the nature of the erodent particles is investigated by calculating erosion rates with Silicon Dioxide (SiO_2) and Silicon Carbide (SiC) as erodent particles. The effect of particle concentration on these materials has also been studied by calculating erosion rates for particle concentrations of C_w = 5 %, 10 %, 15 %, 20 % and 25% with respect to the continuous phase for all pump materials at the fixed speed.

2. MATHEMATICAL MODELLING AND COMPUTATIONAL METHODOLOGY

2.1 Geometry of the industrial centrifugal pump

The centrifugal pump geometry utilized in the present work is a 3-D model conceived in ANSYS R16.0 design modeler and is comprised of three parts, namely the inlet pipe with diameter 69.51 mm, impeller, and a spiral casing as shown in Fig. 1. The impeller consists of six vanes, front shroud, back shroud, vanes, and impeller eye. The eye diameter is 31.991 mm. The impeller at

the inlet has a diameter of 69.51 mm and a width of 13 mm. The outlet at the impeller has a diameter of 139 mm. The casing outlet has a diameter of 20 mm. Carbon steel, stainless steels SS 304 and SS 316 are used as existing industrial pump materials.

2.2 Grid generation of 3-D model

Meshing has been done using the ICEM CFD module of ANSYS R16.0, as shown in Fig. 2 below. The inlet pipe, spiral casing, and impeller consist of tetrahedral, pyramid, and prism elements. The quality of a mesh significantly influences the stability of numerical computation. In order to obtain a high quality grid, mesh quality measures like aspect ratio, orthogonal quality, and skewness are kept within permissible limits. The aspect ratio of an element is the degree of squishiness of an element. It is the ratio of the maximum and minimum distance between cell centroid and face centroid. Skewness is an indication of how close the cell shapes are and with that of the equilateral cell of equivalent volume. High values of skewness may lead to difficulties in the convergence of the solution. A higher orthogonal quality is desired for cells. The orthogonal quality of a cell is considered to be good if it is farther from 0 and the closer it is to 1. The mesh for the model had quality parameters within the acceptable limits with a mean aspect ratio of 4.634, mean orthogonal quality of 0.85 and a mean skewness of 0.69.

2.3 Grid independency test (GIT)

Mesh independence for the simulation was checked by comparing the efficiency of the pump at various grid sizes shown in Fig. 3 and Table.1. The efficiency was not found to vary much after11379287 number of mesh elements.

Therefore, the grid with 11379287 elements is selected.

Table 1. Grid independency test.

No. of elements	Efficiency (%)
2.02751E6	58.42
5.70477E6	77.246
9.04676E6	84.568
1.13793E7	87.874
1.42686E7	87.876
1.82686E7	87.877
2.82686E7	87.878

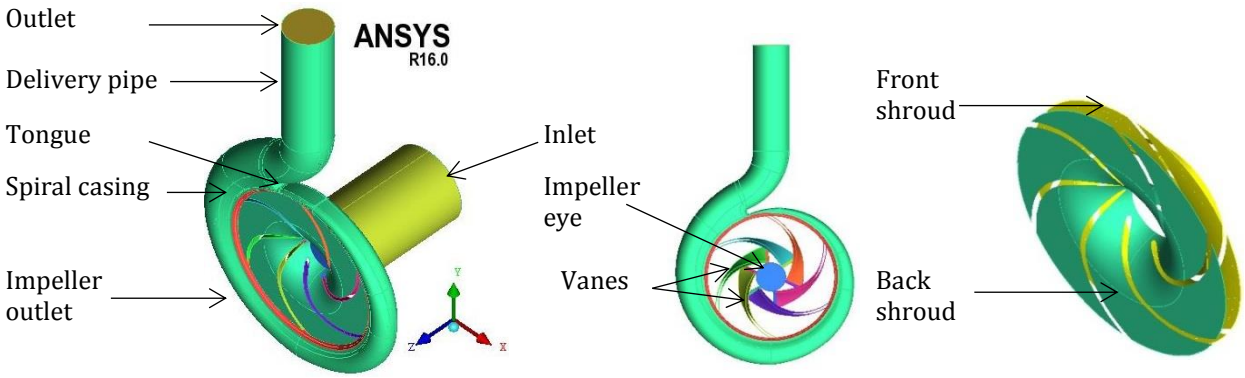

Fig. 1. 3-D model of the centrifugal pump (a) Full Geometry, (b) Vanes assembly, (c) Shroud Assembly.

Fig. 2. Mesh (a) Isometric view of model, (b) Front view of spiral casing, (c) Isometric view of impeller, (d) Front view of impeller.

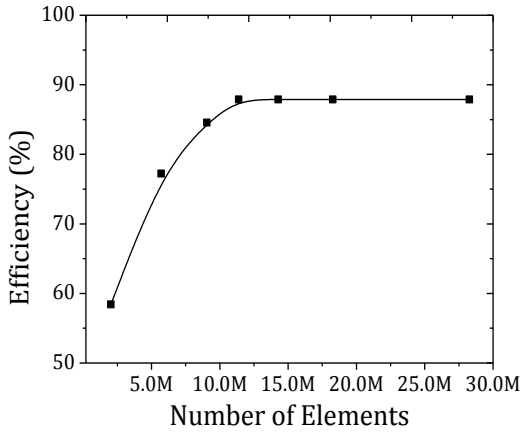

Fig. 3. Grid independency test.

2.4 Computational methodology

Numerical simulation is done using the Euler-Lagrange approach, wherein the fluid flow is the solid erodent particles are treated as resolved by treating it as a continuous phase and discrete particles on account of them having a low volumetric fraction when compared with the continuous phase. The interaction between the continuous phase and the solid phase is modelled using the one-way coupling approach. Unlike the two-way coupling approach wherein the change in momentum of the solid particles is taken as source terms in the momentum equation of the continuous phase, the one-way coupling approach neglects the effect that the particles have on the continuous phase on account of them being low in volume when compared to the continuous phase. The erosion calculation at the wall boundaries is calculated using the erosion model proposed by Oka et al. [33].

2.5 Governing equations for continuous phase

The continuous phase is resolved using the continuum approach, and the standard continuity equation is used for mass conservation. The continuity equation is given in Eq. 1.

$$\frac{\partial \rho}{\partial t} + \nabla \cdot (\rho \vec{v}) = S_m. \quad (1)$$

Where S_m is the term associated with mass addition from a source term and ρ and v are density and velocity of the continuous phase.

The momentum for the continuous phase is resolved using the Reynolds-Averaged Navier-Stokes equation (RANS). The SST k-ω model, which is a two-equation eddy viscosity model is used as a closure model. RANS equation is given in Eq. 2.

$$\frac{\partial(\rho\overline{u_i})}{\partial t} + \frac{\partial}{\partial x_j}\left(\rho\overline{u_\iota}\,\overline{u}_j + \rho\overline{u_i{'}u'_j}\right) = -\frac{\partial \overline{p}}{\partial x_i} + \frac{\partial}{\partial x_j}\left[\mu\left(\frac{\partial \overline{u_\iota}}{\partial x_j}\frac{\partial \overline{u}_j}{\partial x_i}\right)\right]. \quad (2)$$

$(\rho\overline{u_i{'}u'_j})$ are the Reynolds's stresses. The Reynold's stresses as per Boussinesq's approximation is given in Eq. 3.

$$-\rho\overline{u_i u_j} = -\rho\frac{2}{3}k\delta_{ij} + \mu_t\left(\frac{\partial \overline{u_\iota}}{\partial x_j} + \frac{\partial \overline{u}_j}{\partial x_i}\right). \quad (3)$$

Where μ_t is turbulent viscosity given by:-

$$\mu_t = \rho\frac{k}{\omega}.$$

The transport equations for k and ω as per the SST k-ω model are given in Eq. 4 and Eq. 5.

$$\frac{\partial(\rho\omega)}{\partial t} + \frac{\partial(\rho U_j\omega)}{\partial x_j} = \frac{\gamma}{v_t}P_k - \beta\rho\omega^2 + \frac{\partial}{\partial x_j}\left(\Gamma_\omega\frac{\partial \omega}{\partial x_j}\right) + (1-F_1)2\rho\sigma_{\omega 2}\frac{1}{\omega}\frac{\partial k}{\partial x_j}\frac{\partial \omega}{\partial x_j}. \quad (4)$$

$$\frac{\partial(\rho k)}{\partial t} + \frac{\partial(\rho U_j k)}{\partial x_j} = \widetilde{P_k} - \beta^*\rho\omega k + \frac{\partial}{\partial x_j}\left(\Gamma_k\frac{\partial k}{\partial x_j}\right). \quad (5)$$

$$\text{with, } \Gamma_k = \mu + \frac{\mu_t}{\sigma_k}, \Gamma_\omega = \mu + \frac{\mu_t}{\sigma_\omega},$$

$$P_k = \tau_{ij}\frac{\partial(U_i)}{\partial x_j}, \widetilde{P_k} = min(P_k; c_1\varepsilon).$$

where, Γ_k and Γ_ω are effective diffusivities and taken C_1=10, β*=0.09. F_1 is the blending function which helps in resolving the near wall flow with the k-ω model and the rest of the flow by k-ε and is given in Eq. 6.

$$F_1 = \tanh(arg_1^4). \quad (6)$$

Where, $arg_1 \min\left(max\left(\frac{\sqrt{k}}{\omega y\,\beta^*}; \frac{500\nu}{y^2\omega}\right); \frac{4\rho k\sigma_{\omega_2}}{y^2 CD_{k\omega}}\right)$.

$\sigma_{\omega 1}$ = 2, $\sigma_{\omega 2}$ = 1.168.

$$CD_{k\omega} = \max\left(2\rho\sigma_{\omega_2}\frac{1}{\omega}\frac{\partial k}{\partial x_j}\frac{\partial \omega}{\partial x_j}; 1.0e^{-10}\right).$$

The SST k-ω model introduces an upper limit for turbulent stress in boundary layers and as a result μ_t is given in Eq. 7.

$$\mu_t = \rho\frac{a_1 k}{max(a_1\omega; \sqrt{2}\,S\cdot F_2)}. \quad (7)$$

Where a_1=0.31, and F_2 is blending function given by:

$$F_2 = \tanh(arg_2^4),\ arg_2 = \left(2\frac{\sqrt{k}}{\omega y\,\beta^*}; \frac{500\nu}{y^2\omega}\right).$$

2.6 Governing equations for dispersed phase

The dispersed phase is resolved using the Lagrangian approach. The Eq. 8 for the solid particle therefore are:

$$\frac{d\overrightarrow{u_p}}{dt} = \frac{\vec{u}-\overrightarrow{u_p}}{\tau_r} + \frac{\vec{g}(\rho_p-\rho)}{\rho_p} + \vec{F}\,. \quad (8)$$

Where $\vec{F}$ is an additional acceleration accounting for forces such as gravity forces, virtual mass force etc. $\frac{\vec{u}-\overrightarrow{u_p}}{\tau_r}$ is the drag force per particle mass and τ_r is the particle relaxation time given by: -

$$\tau_r = \frac{\rho_p d_p^2}{18\mu}\frac{24}{C_d\,Re}.$$

Where *Re* is the Reynolds number relating to the relative velocity of the particle with respect to the flow velocity.

$$Re = \frac{\rho d_p\,|\vec{u}_p-\vec{u}|}{\mu}.$$

2.7 Erosion modelling

The model proposed by Oka et al. [34] was used for calculating the erosion rate at the walls. The erosion rate at the walls is given in Eq. 9.

$$E(\alpha) = \frac{1}{10^9}\,\dot{m}\rho_m\,(sin\,\alpha)^{n_1}\,(1 + H_v(1 - sin\,\alpha))^{n_2}\,K(aH_v)^{bk_1}\left(\frac{v}{v'}\right)^{k_2}\left(\frac{d}{d'}\right)^{k_3}. \quad (9)$$

Where , E(α) is the rate of erosion in kg/s for a particle impact angle of α, K_1 is a function of particle properties like angularity, K_2 is the velocity constant which is independent of the particle diameter but is dependent on the erodent particle and the material hardness, K_3 is the particle size constant independent of the particle velocity but dependent on the erodent particle and material hardness, *a* and *b* are the load relaxation properties of the material and n_1 and n_2 are constants which are a function of the material hardness*(H_v)* and shape of erodent particles. v and d stand for the velocity of impact and particle diameter, whereas v' and d' indicate the standard values for the same, which are utilized for erosion damage correlations in the experiments. Experimentally obtained exponents of v and d can also be used for dimesionless terms of (*v/v'*) and (d/d'). All constants are reproduced from the Oka et al. [33] and given in Table 2.

2.8 Boundary conditions, solution control and convergence

ANSYS fluent R16.0 was used for the numerical simulation. The semi-implicit method for pressure linked equations was utilized for solving the pressure-velocity coupling. The convective terms and diffusion terms are solved using the second order upwind scheme and second order central differencing scheme, respectively. For the continuous phase, the mass flow rate was specified at the inlet, and the outlet was considered a pressure outlet. The impeller was set at a speed of 1450 rpm, which was the design condition for the pump. The casing was set as a stationary wall with no-slip boundary condition, and the blades were set as moving walls moving at the speed of the impeller. Interfaces were specified, firstly between the inlet pipe and the impeller inlet and secondly between the impeller outlet and the casing inlet. The SiO_2 and SiC erodent particles were treated as a discrete phase. These particles were assumed to be of a uniform diameter of 106 μm and were released from the pipe inlet and escaped the flow domain from the outlet. The particles were set to have perfectly elastic collisions with the surface of the casing and the blades. The erosion values at the casing, vane, front shroud, and back shroud were calculated using a user defined function, which utilized the model given by Oka et al. [33] and as mentioned in the equation above.

Table 2. Different constants for the erosion modeling (Oka et al. [33,34]).

Pump material	K	K_1	K_2	K_3	n_1	n_2	a	b	Hv (GPa)	v' (m/s)	d' (μm)	Density (kg/m³)	Erodent
CS	65	-0.12	2.32	0.19	0.74	1.82	0.30	0.604	1.34	104	326	7700	SiO_2
CS	45	-0.05	3.07	0.19	0.74	2.09	0.30	0.604	1.34	99	326	7700	SiC
SS 304	65	-0.12	2.31	0.19	0.82	0.88	1.18	0.028	2.9	104	326	7890	SiO_2
SS 304	45	-0.05	3.28	0.19	0.82	0.96	1.18	0.028	2.9	99	326	7890	SiC
SS 316	65	-0.12	2.32	0.19	0.74	1.78	1.19	0.056	1.37	104	326	7730	SiO_2
SS 316	45	-0.05	3.08	0.19	0.74	2.04	1.19	0.056	1.37	99	326	7730	SiC

CS= Carbon Steel, SS= Stainless Steel

Table 3. Various hydraulic parameters of the pump at different regimes.

Discharge (cumec)	Inlet total pressure (Pa)	Outlet total pressure (Pa)	Torque (N-m)	Input power (Watt)	Output power (Watt)	Head (m)	Hydraulic efficiency (%)
0.0035	101793	162657	1.64	248.72	213.02	6.21	85.64
0.0036	101818	161939	1.66	253.33	216.43	6.12	85.43
0.0037	101847	161378	1.68	255.79	220.26	6.06	86.11
0.0038	101886	160047	1.70	258.48	221.01	5.92	85.50
0.0039	101903	159946	1.73	262.66	226.36	5.91	86.17
0.0040	101924	159879	1.75	267.11	231.82	5.90	86.78
0.0042	101980	159399	1.80	274.42	241.15	5.85	87.87
0.0043	102033	158638	1.83	278.58	243.40	5.77	87.37
0.0044	102084	156567	1.85	281.82	239.72	5.55	85.06
0.0045	102149	156076	1.89	286.98	242.67	5.49	84.55

2.9 Validation of computational methodology

For the validation of the computational methodology explained above the experimental heads developed at different discharge by water handling industrial centrifugal pump at designed speed of 1450 rpm were chosen which were provided by Kirloskar Pvt. Ltd., Pune, Maharashtra, India. Details of all the data are given in Table 3.

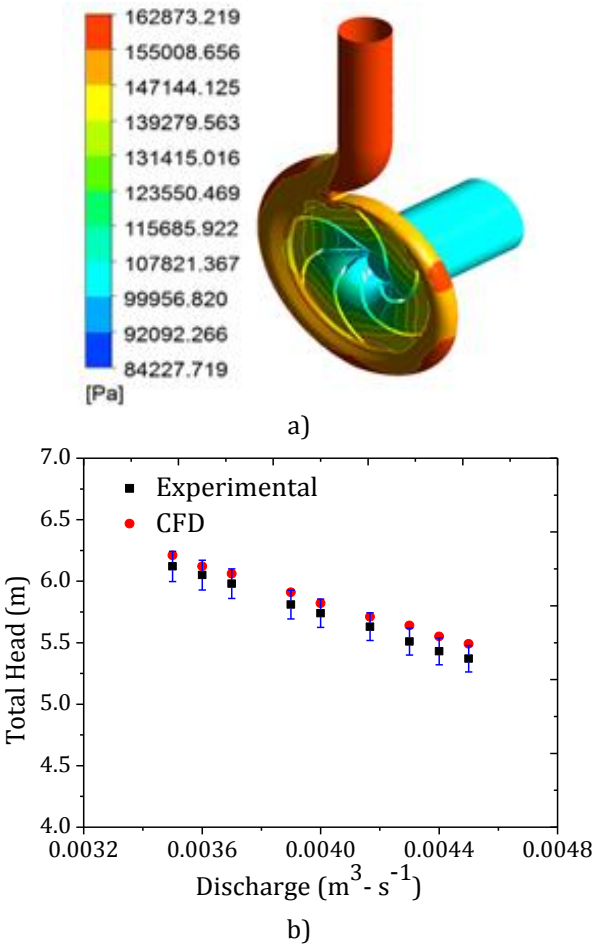

Fig. 4. (a) Pressure contours for 3d model, (b) Validation of head.

These heads were compared against the results obtained by the numerical strategy of the pump, as mentioned above using ANSYS fluent R16.0. The results were found to be in good agreement (±2 % deviation) with the experimental results provided, as shown in Fig. 4b. Corresponding pressure contours have also been shown in Fig. 4a for the sake of clarity.

3. RESULTS AND DISCUSSIONS

The erosion values for pump casing, blades, and hub are determined using computational methodology as explained in section 2.0 above at a designed speed of 1450 rpm and is summarized in Fig. 5. Analysis of the results so obtained has been explained in the subsequent sections.

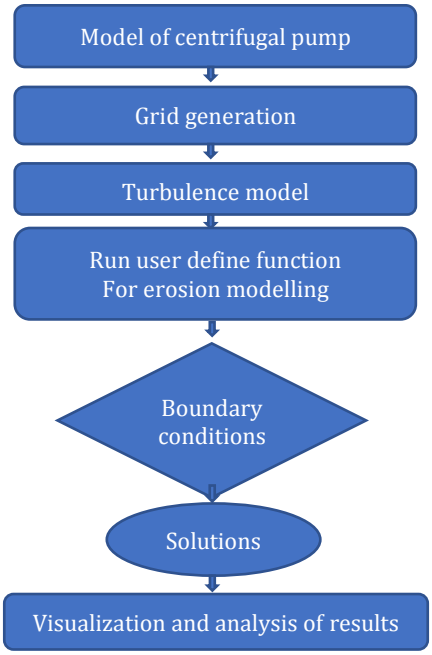

Fig. 5. Flow Chart of the adopted computational methodology.

3.1 Erosion density distribution along various components of the pump

Before analyzing the pattern of erosion wear due to solid particles, it is inevitable to see how the particles are traversing inside the pump along with the fluid. Thus, particle tracks for each of the cases studied in the current work have been shown in Figs. 6a and 6b.

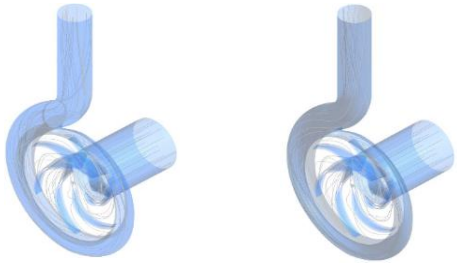

(a) (b)

Fig. 6. Solid particle density distribution for SiC at (a) C_w = 5 %, (b) C_w = 25 %.

These shall be analyzed in subsequent sections for each component of the pump. The erosion rate has been calculated using the one-way coupling method. Since the continuous phase has been accurately resolved, the erosion rate calculated in the following sections would only be dependent on erosion parameters such as type of pump material and the type of erodent material used and the concentration of the erodent. The particle track as shown in Fig. 6 depicts that the number of particles impacting with the pump increases whenever there is a change in the direction of the flow of fluid.

3.2 Erosion at pump casing

The average values of erosion wear at pump casing have been calculated separately from the computational methodology at various concentrations ranging from 5 % to 25 % for both of the erodent material (SiO_2 and SiC) on Carbon steel, Stainless steel 304 and Stainless steel 316 pump materials separately. The results so obtained have been drawn in Fig. 7. The figure shows that as the concentration of particles increases, the erosion rate increases almost linearly. This is obvious since with the increase in a number of particles due to an increase in the concentration of solid particles, the overall contact surface area of particles available for wear increases. These results are consistent with the results mentioned in Noon & Kim [5], Gandhi et al. [9] and Rawat et al. [10], Gupta et al. [35] for the various concentrations of solids.

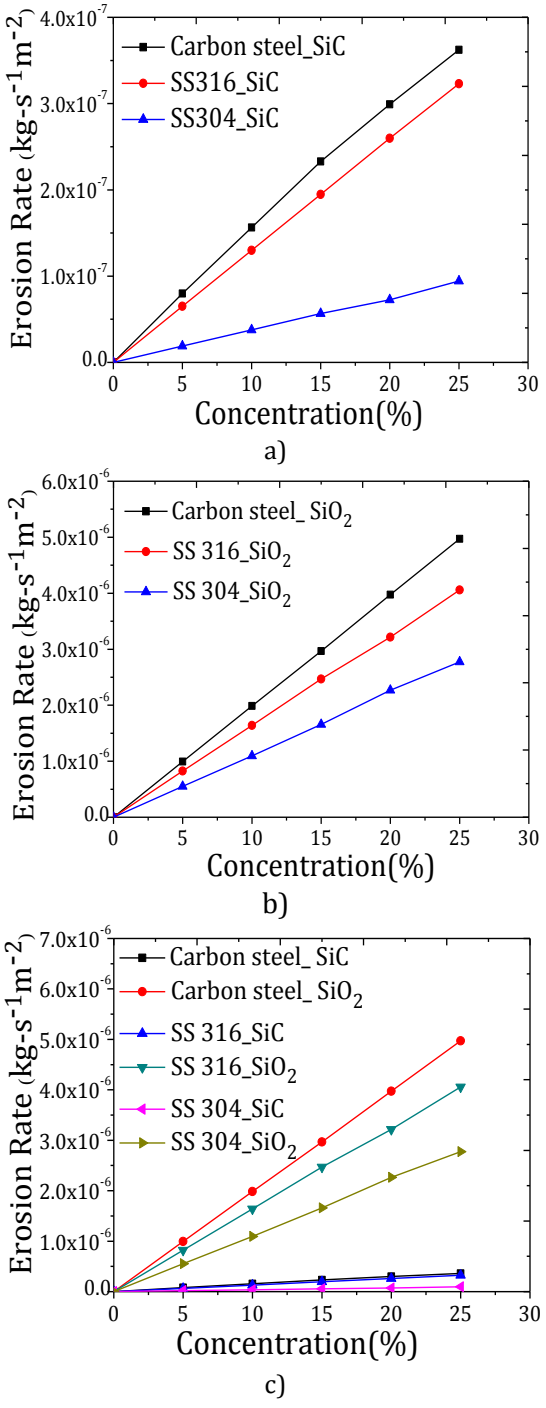

Fig. 7. Erosion rate in spiral casing of carbon steel, SS316 and SS304, (a) For erodent particle SiC, (b) For erodent particle SiO_2, (c) Comparison of erosion rate for erodent particle SiC and SiO_2.

Further, the change of erodent material and target material (casing material) affects the amount of erosion wear. For the same erodent material, the rate of increase in erosion wear is

higher in the case of Carbon steel than SS 316 and SS 316 has a higher erosion rate than SS 304. It is essential to mention that the toughness of Carbon steel is lower than SS316 and SS304 both, whereas the toughness of SS316 is lesser than SS304. Thus, the behaviors of erosion wear on Carbon steel can be easily explained, but in the case of SS316 and SS304, not only the toughness but also the way the particles interact with the surfaces also play an important role. Values of n_1 and n_2 are higher in the case of SS316 than SS304, Table 1, Oka et al. [33,34]. Figure 7c reveals that the erosion wear for SiO_2 is higher than SiC on all three target materials since the hardness of SiO_2 is higher than SiC. The experimental values shown in the above graphs are average values for the casing. For a detailed analysis of erosion on the pump casing at different locations, the erosion rate contours have been plotted in Figs. 8 and 9. Careful analysis of the figures (Figs. 8 and 9) reveals that the erosion rate values for the casing. For a detailed analysis of erosion on the pump casing at different highest at the narrowest part of the casing regardless of the erodent used or the concentration of the erodent. This is due to the fact that due to the narrower flow passage area, the particle velocities may be highest causing, more wear. The particles tracks are shown in Fig. 6 also suggest and depict the concentration of particles in the narrower zone of the casing. From Figs. 8 and 9, the contours for the spiral casing, the erosion rate is found to be nearly uniform in the rest of the flow passage except for the regions where the flow direction is changed suddenly. The sudden change of direction causes the secondary flow of particles and a centrifugal action on the particles providing relatively higher energies to the particles, which results in relatively more wear than the rest of the part of the spiral casing.

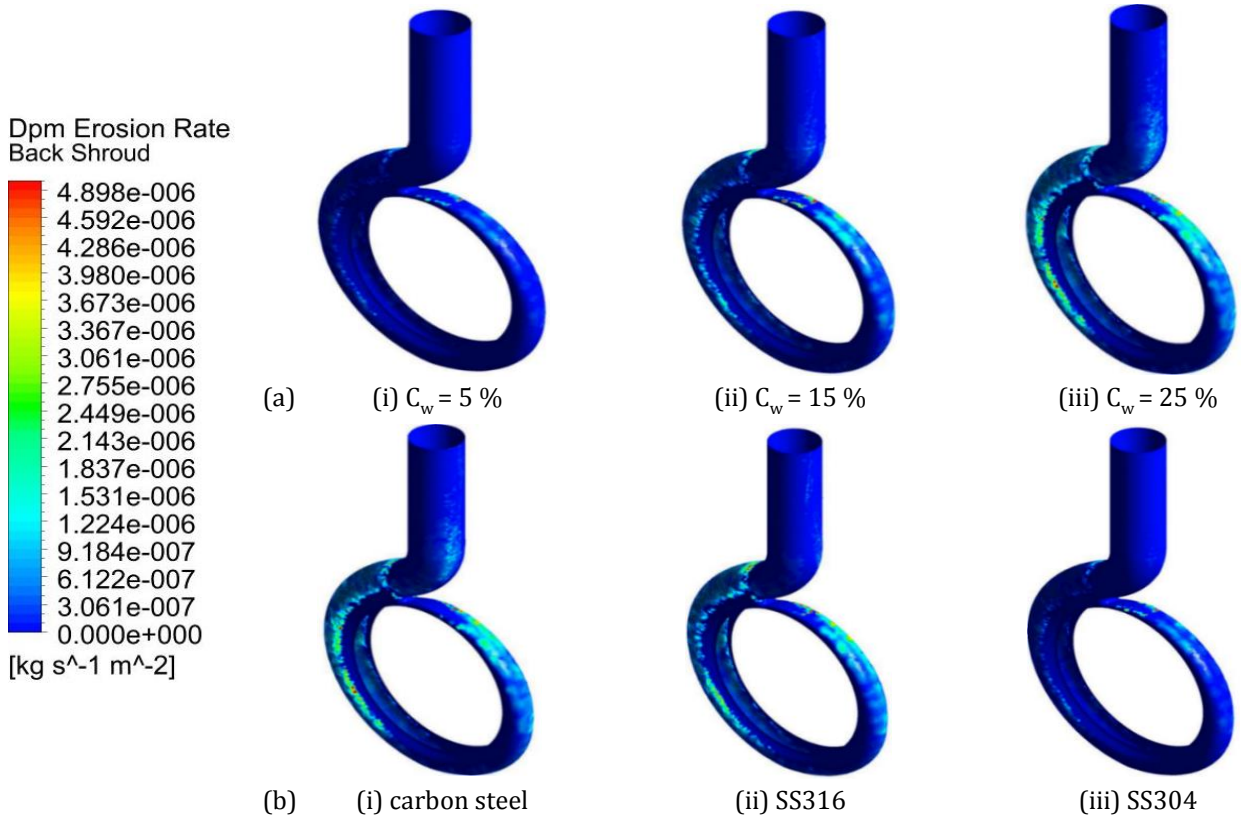

Fig. 8. Erosion rate contours at spiral casing with SiC as erodent for (a) Carbon Steel at different concentrations, (b) Erosion contour for carbon steel, SS316 and SS304 at C_w = 25 % .

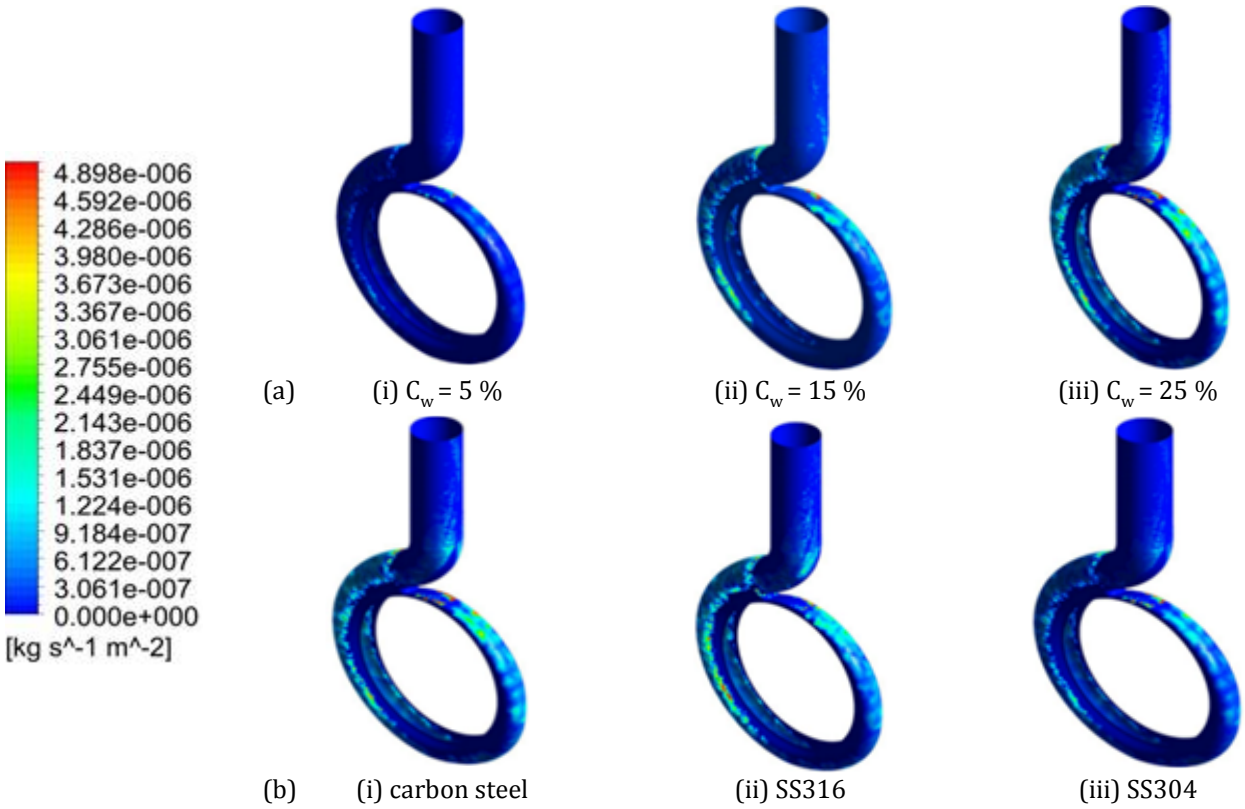

Fig. 9. Erosion rate contours at spiral casing with SiO_2 as erodent (a) For carbon steel at different concentrations, (b) Erosion contour for carbon steel, SS316 and SS304 at C_w = 25 %.

3.3 Erosion wear on impeller vanes

The erosion wear variation rate at the vanes of the pump has the same patterns as that for the pump casing i.e., erosion wear increases as the concentration increases, and SiO_2 creates more wear than SiC (Fig. 10c). Also, Carbon Steel, SS 316 and 304 observe erosion wear due to erodent materials in increasing fashion (Fig. 10). Whereas, the erosion in the blades occurs primarily at the tip of the blades and at the top of the blades (Figs. 11 and 12), where the axial flow from the inlet pipe is turned to the radial outward flow in the blade passage.

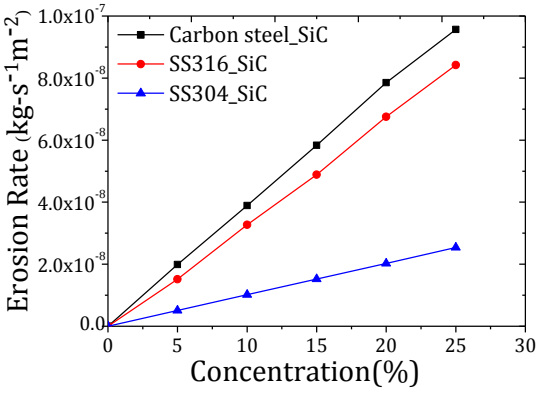

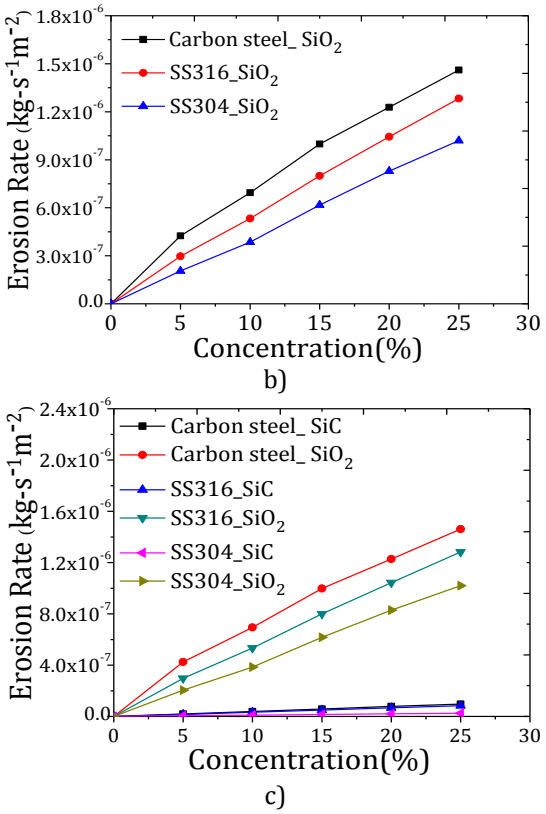

Fig. 10. Erosion rate in vane of carbon steel, SS316 and SS304 (a) For erodent particle SiC, (b) For erodent particle SiO_2, (c) Comparison of erosion rate for erodent particle SiC and SiO_2.

To visualize this aspect better, an enlarged view of vanes has been shown in Fig. 11d. The erosion rate on the suction side is also found to be more than the erosion rate on the pressure side of the blade as the velocities of the fluid is higher on the suction side.

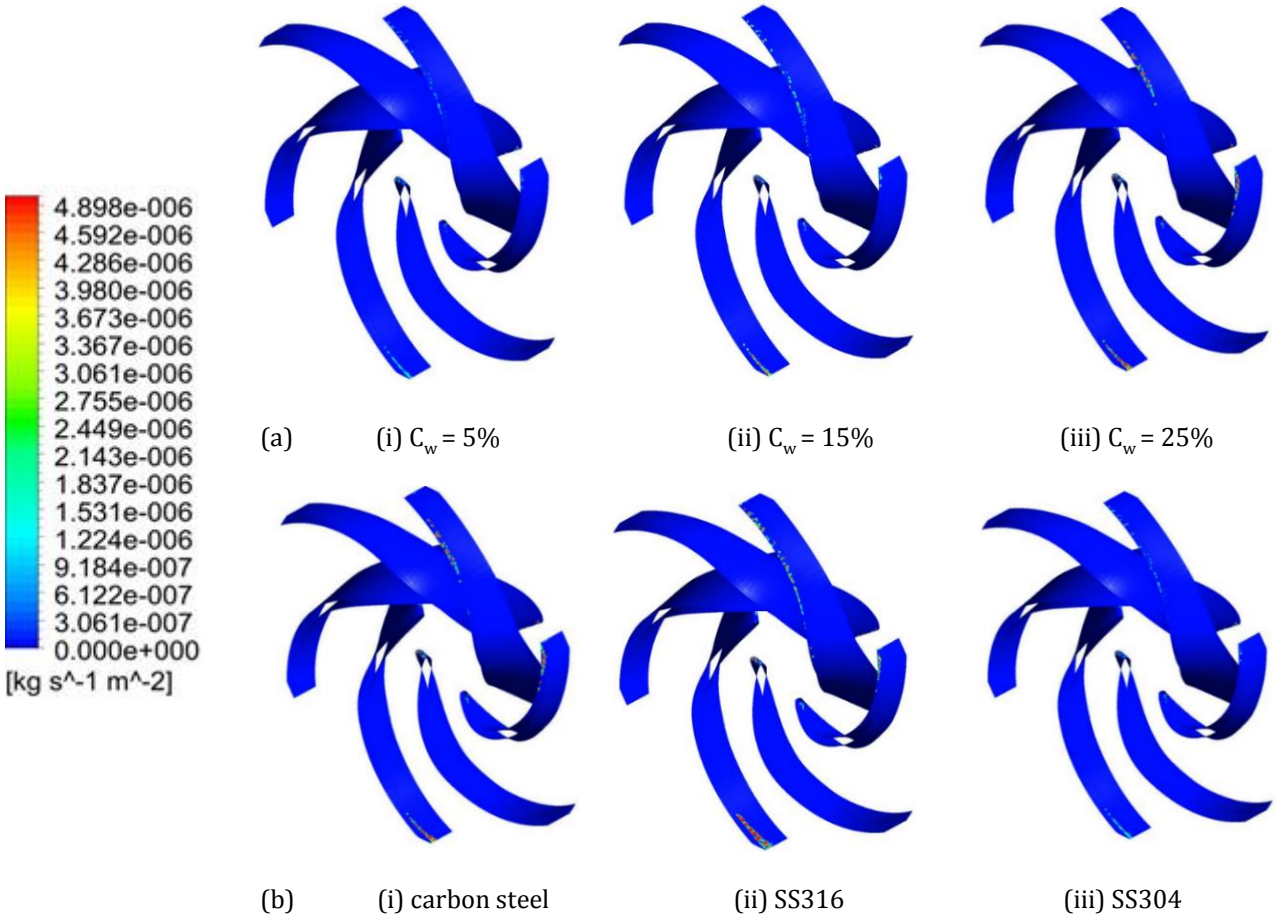

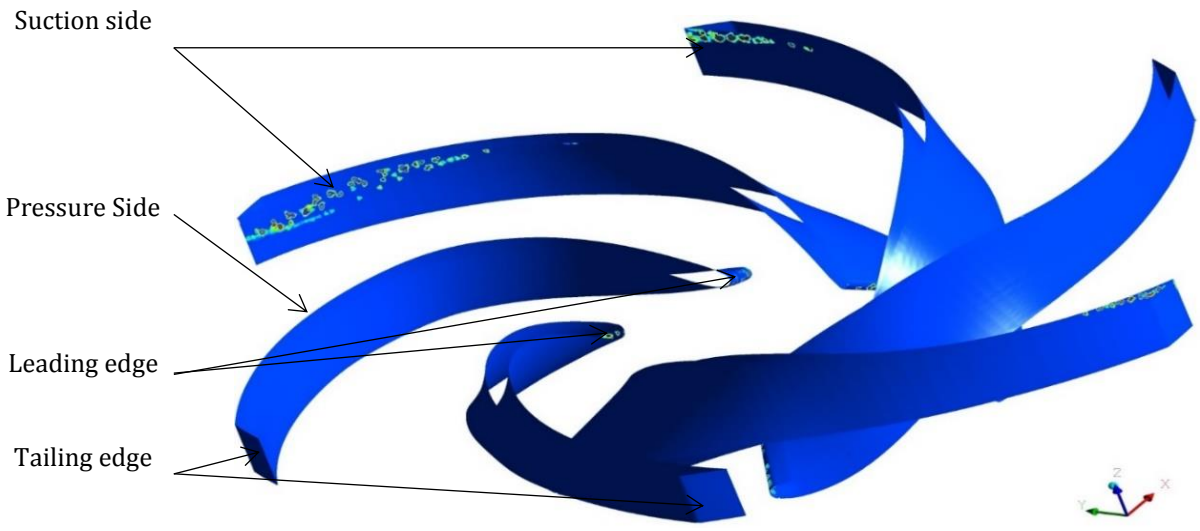

(c) Enlarged view of vane depicting wear incurred at C_w=25 % for carbon steel for SiC erodent particle

Fig. 11. Erosion rate contours at the vanes with SiC as erodent (a) For carbon steel at different concentrations, (b) Erosion contour for carbon steel, SS316 and SS304 at C_w = 25 %, (c) Enlarge view of vanes.

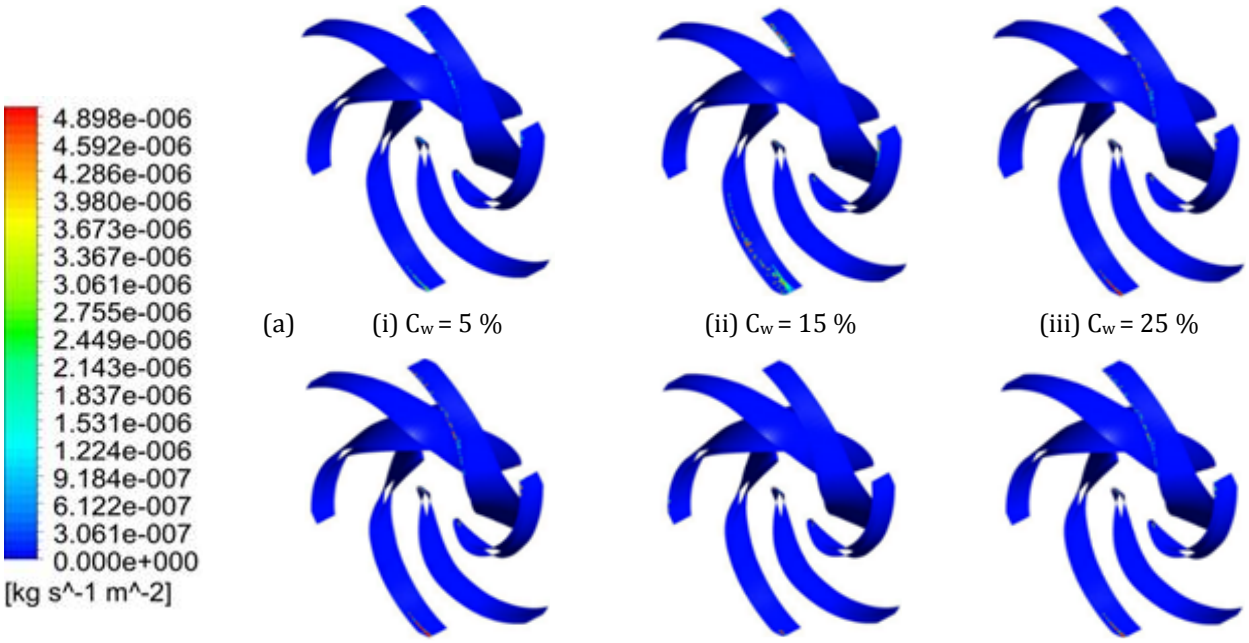

Fig. 12. Erosion rate contours at the vanes with SiO_2 as erodent for (a) Carbon Steel at different concentrations, (b) Erosion contour for carbon steel, SS316 and SS304 at C_w =25 %.

3.4 Erosion wear at impeller shrouds

The erosion wear variation rate at the front shroud and back shroud of the pump has the same patterns as that for the pump casing i.e., erosion wear increases as the concentration increases, SiO_2 creates more wear than SiC (Figs. 13c and 14c). Also, Carbon Steel, SS316, and 304 observe erosion wear due to erodent materials in an increasing fashion (Fig. 13a and Fig. 14b respectively). As far as the overall average wear at the shrouds is concerned, the observations are no different than those which were observed in case of the casing and the vanes. But, the erosion rate at the front shroud is found to be maximum at the outer edge of the shroud regardless of the pump material or erodent material, as can be seen from Fig. 15 to Fig. 18. The reason for this is the same as was for vanes. Due to increased velocity at the outer edges, the erosion is more whereas the back shrouds receive very fewer solids particles than the front shroud. This causes less wear at the back shroud than a front shroud.

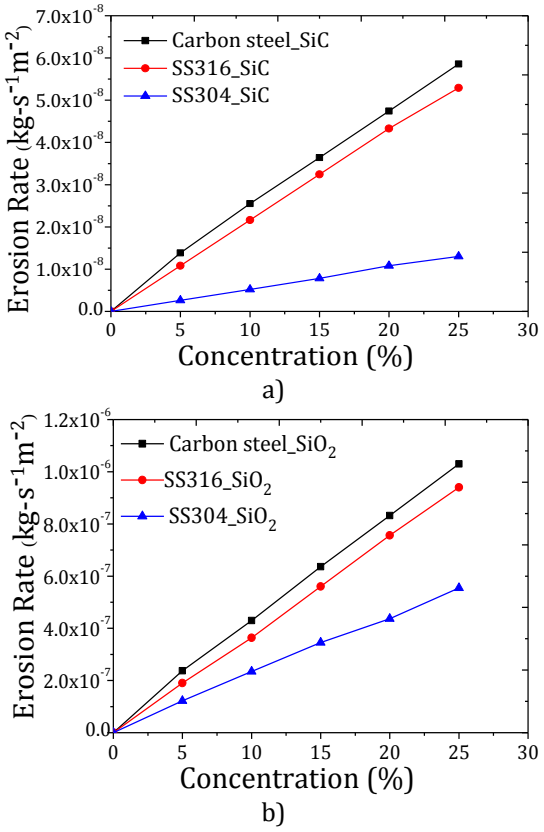

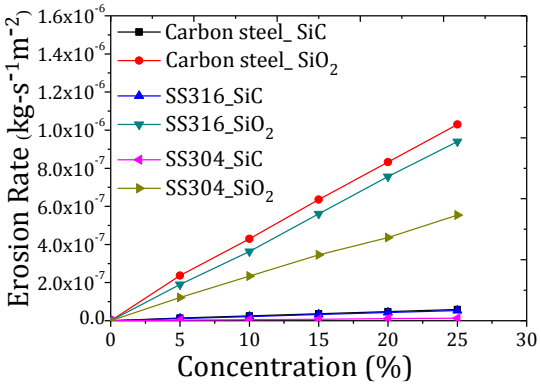

c)

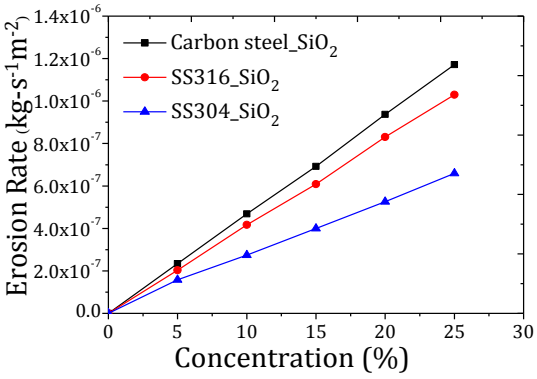

b)

Fig. 13. Erosion rate in front shroud of carbon steel, SS316 and SS304 (a) For erodent particle SiC, (b) For erodent particle SiO_2, (c) Comparison of erosion rate for erodent particle SiC and SiO_2.

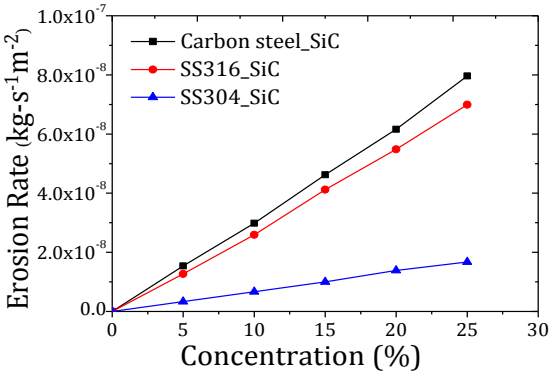

a)

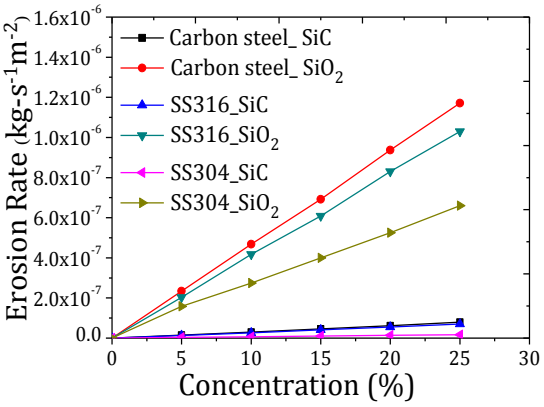

c)

Fig. 14. Erosion rate in back shroud of carbon steel, SS316 and SS304 (a) For erodent particle SiC, (b) For erodent particle SiO_2, (c) Comparison of erosion rate for erodent particle SiC and SiO_2.

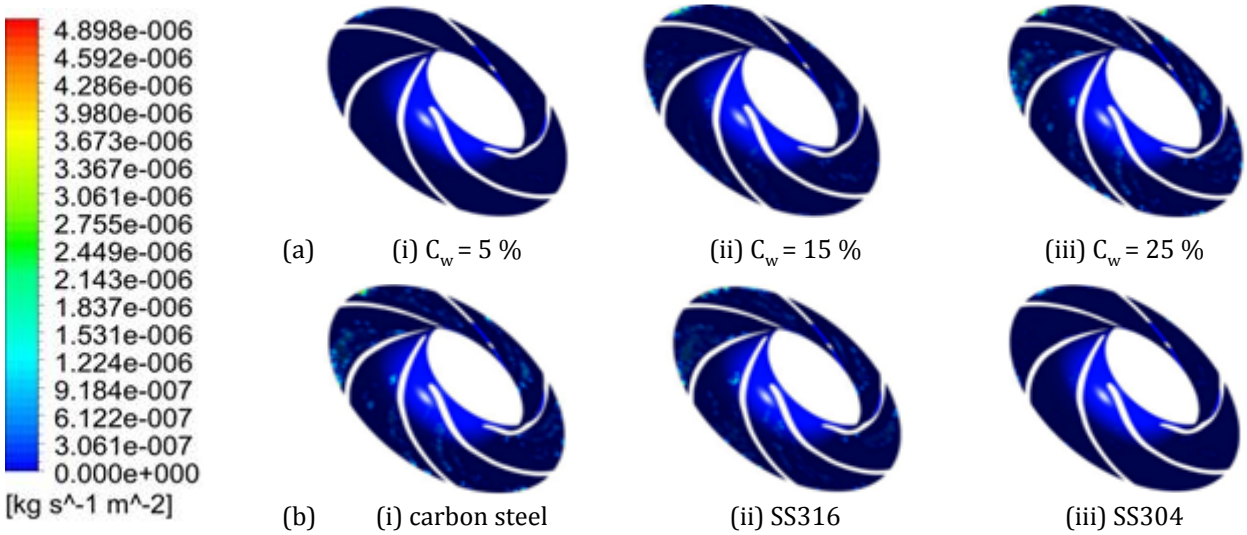

Fig. 15. Erosion rate at front shroud with SiC as erodent for (a) Carbon Steel at different concentrations, (b) Erosion contour for carbon steel SS316 and SS304 at C_w = 25 %.

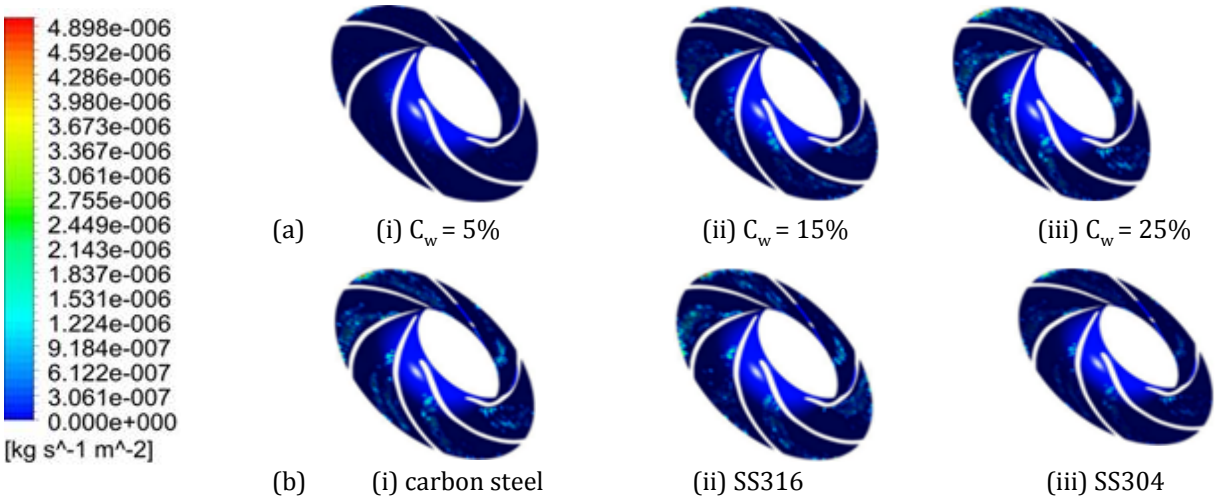

Fig. 16. Erosion rate at front shroud with SiO_2 as erodent for (a) Carbon Steel at different concentrations, (b) Erosion contour for carbon steel SS316 and SS304 at C_w = 25 %.

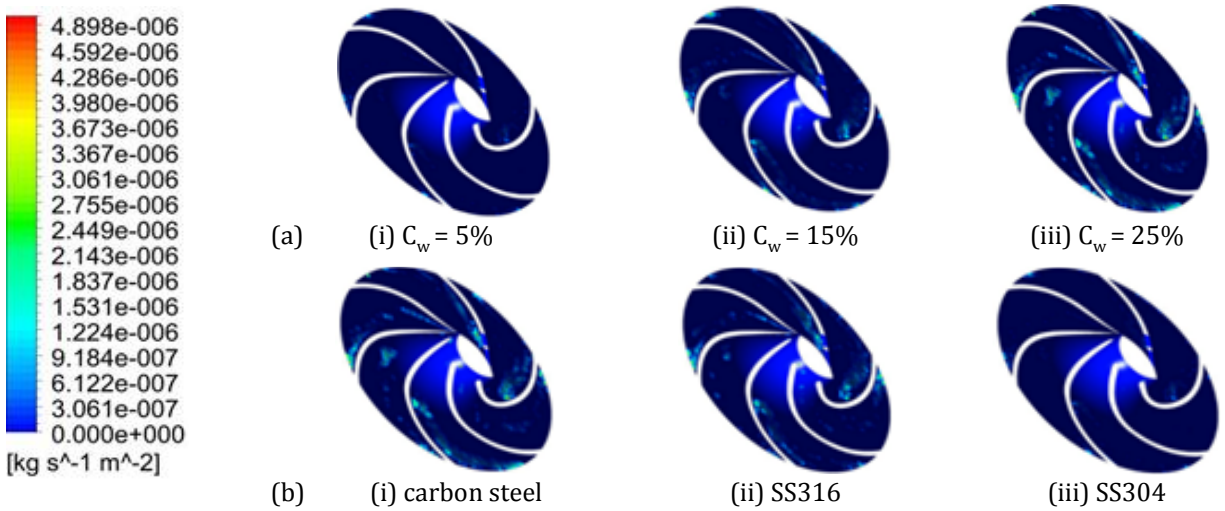

Fig. 17. Erosion rate at Back Shroud with SiC as erodent (a) For carbon steel at different concentrations, (b) Erosion contour for carbon steel, SS316 and SS304 at C_w =25 %.

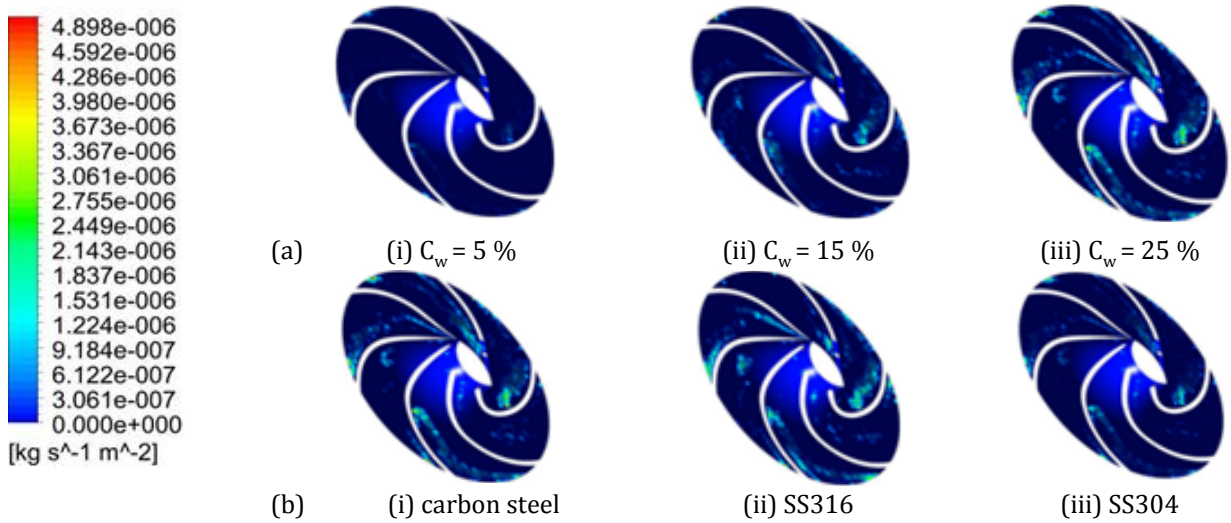

Fig. 18. Erosion rate at Back Shroud with SiO_2 as erodent (a) For carbon steel at different concentrations, (b) Erosion contour for carbon steel, SS316 and SS304 at C_w =25 %.

3.5 Comparison of erosion wear at different components of the pump

Apart from the individual analysis of various components of the pump, a cumulative comparison of erosion wear incurred at various components of the pump has also been carried out and graphs between erosion wear, and concentrations have been drawn in Figs. 19-21 for every component for all pump material and erodent particles considered in the study. The figures show that the pump casing receives maximum wear than the rest of the components. At the highest concentration of 25 %, the casing receives around 7-8 times higher wear than vanes and shrouds, which is due to the relatively more interaction of the dispersed phase with the casing while the pumping action is taking place. Whereas, the vanes receive relatively higher erosion wear than the shrouds as shrouds interact with the solid's particles least. But in comparison to the casing, both of the components can be considered to receive almost the same amount of wear for all cases of target materials of pump and erodent particles.

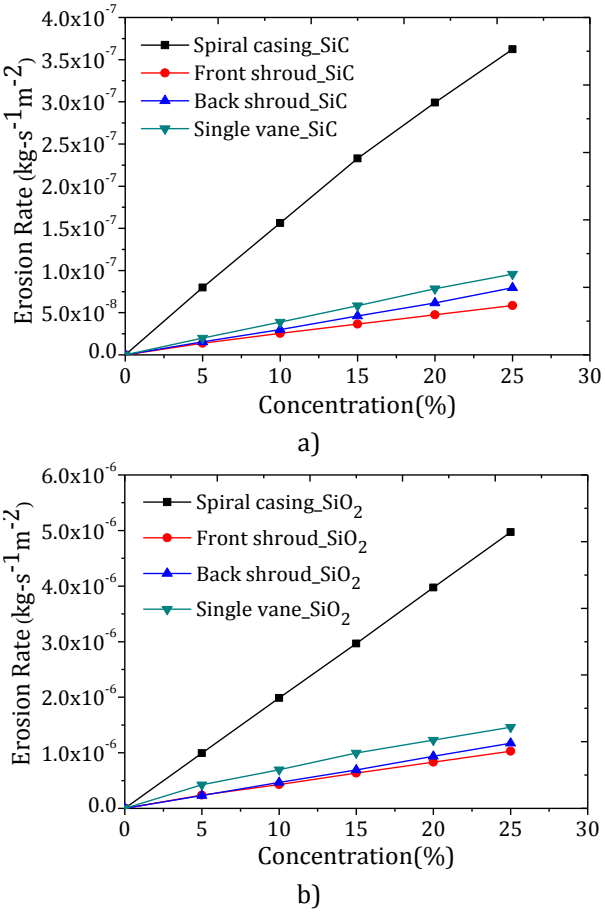

Fig. 19. Erosion rate of different parts of pump for carbon steel (a) SiC erodent particle, (b) SiO_2 erodent particle.

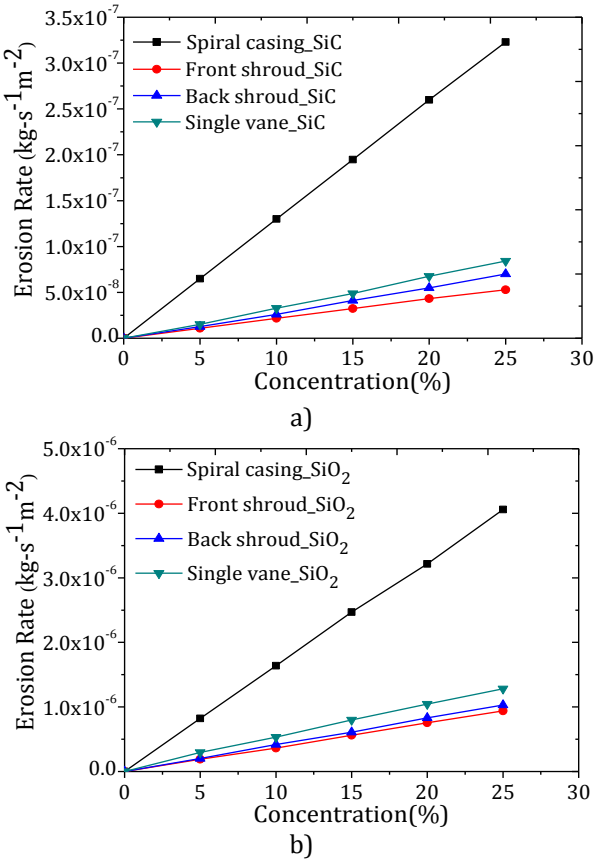

Fig. 20. Erosion rate of different parts of pump for SS316 (a) SiC erodent particle, (b) SiO_2 erodent particle.

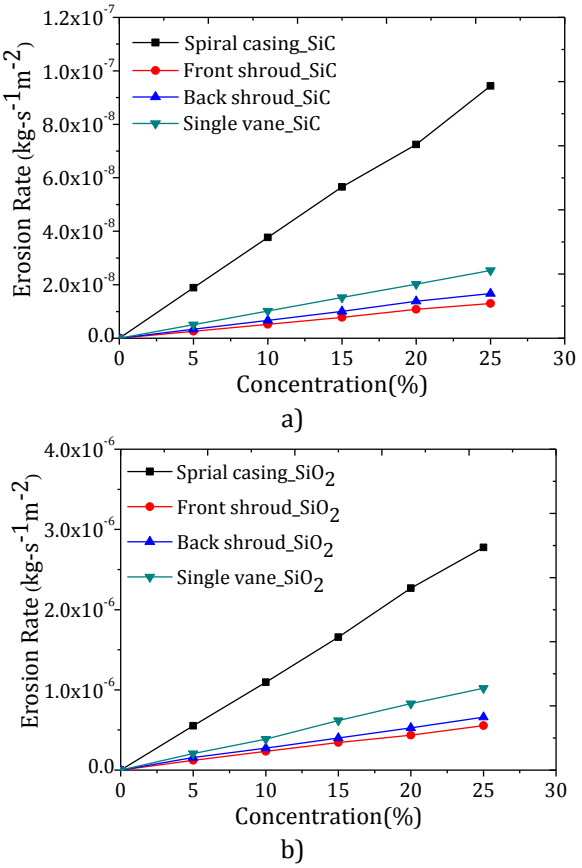

Fig. 21. Erosion rate of different parts of pump for SS304 (a) SiC erodent particle, (b) SiO_2 erodent particle.

3.6 Effect of particle size on erosion wear

Further to understand the effect of particle size of erosion wear, a limited study is conducted on different target materials of Carbon steel, SS316 and SS304 for the different particle sizes of SiO_2 (50-250 μm) at fixed C_w = 10%. The results so obtained have been drawn in Fig. 22.

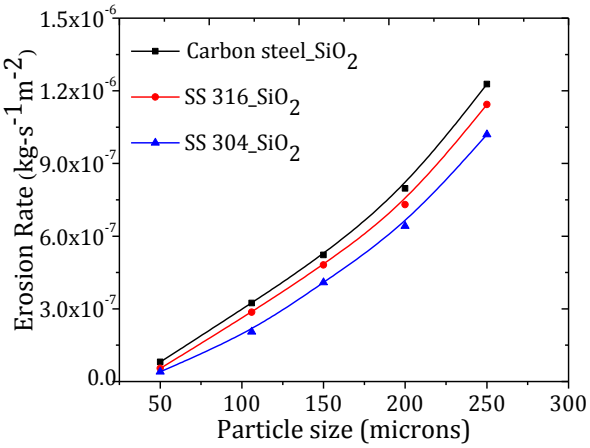

Fig. 22. Effect of solid particle size on single vane for SiO_2 at C_w = 10 % and V = 10 m/s.

It is clearly seen that as the particle size increases the amount of erosion wear also increases for all target materials. The results so obtained are consistent with Gandhi et al. [9] and Zhong and Minemura [11]. Whereas, the effect of particle size is more pronounced for Carbon steel than the rest of the two target materials on account of its lesser toughness.

4. CONCLUSIONS

In this work, a comparative erosion wear study for different pump materials has been carried out through comprehensive numerical hydrodynamic analyses. The results are found to be consistent with many researches available in literature [2,6-8]. The following are the major conclusions that can be made from the present work.

- The numerical investigation developed in the current work predicts that the erosion rate at the locations in the pump parts where the flow suddenly changes direction is significantly higher than that at nearby locations.
- It is found that for all the three common steel, the erosion at the spiral casing is higher than at any other component of the pump. Thus, the design of the casing is more critical than the other components as far as erosion wear to save overall cost is concerned.
- The vanes of the pumps observe more variation of wear from the tip to the top for all the three steel. Thus, these components are to be designed more carefully by the designers of such pumps.
- The study also depicts that the edges of the front shrouds are to be designed carefully for erosion wear as they receive more wear.
- All pump parts showed that SS304 is the most suitable material for pumps handling sand slurries to receive minimum wear in hydraulic power plants.
- The steels investigated in the current work also showed more resistance to erosion due to SiC when compared to SiO_2 at all pump locations.

Acknowledgement

The authors would like to acknowledge the TEQIP-III for funding the project. Authors also like to thank Kirloskar Brothers Limited, Pune, India, who not only supplied the experimental data for the current work but also pointed out the problems faced by their pumps. This gave the authors a motivation to work towards minimization of the associated wear. In particular, the contribution of Dr. S. N. Shukla in terms of technology transfer of the knowledge is much appreciated.

REFERENCES

[1] B. Kishor, G.P. Chaudhari, S.K. Nath, *Slurry erosion of thermo-mechanically processed 13Cr4Ni stainless steel*, Tribology International, vol. 93, pp. 50–57, 2016, doi: 10.1016/j.triboint.2015.08.048

[2] S. Gupta, A. Khandelwal, A.K. Ghose, I. Chakrabarty, *Slurry Erosion Behavior of Destabilized and Deep Cryogenically Treated Cr-Mn-Cu White Cast Irons*, Tribology in Industry, vol. 38, no. 4, 486-495, 2016.

[3] S.R. More, D.V. Bhatt, J.V. Menghani, *Study of the Parametric Performance of Solid Particle Erosion Wear under the Slurry Pot Test Rig*, Tribology in Industry, vol. 39, no. 4, 471-481, 2017, doi: 10.24874/ti.2017.39.04.06

[4] S. Aribo, I. Adedapo, C. Nwogwugwu, O. Olaniran, A. Olaseinde, O. Ige, P.A. Olubambi, *Erosion-corrosion Behaviour of Dual Phase Medium Carbon Steel using a Designed Slurry Pot*, Tribology in Industry, vol. 40, no. 2, 239-246, 2018, doi: 10.24874/ti.2018.40.02.07

[5] A.A. Noon, M.-H. Kim, *Erosion wear on centrifugal pump casing due to slurry flow*, Wear, vol. 364-365, pp. 103-111, 2016, doi: 10.1016/j.wear.2016.07.005

[6] R. Tarodiya, B.K. Gandhi, *Numerical simulation of a centrifugal slurry pump handling solid-liquid mixture: Effect of solids on flow field and performance*, Advanced Powder Technology, vol. 30, iss. 10, pp. 2225-2239, 2019, doi: 10.1016/j.apt.2019.07.003

[7] V. Gautam, A. Kumar, L. Prasad, V.K. Patel, *An Experimental Investigation on Slurry Erosion Wear Characteristics of Brass Alloy*, Materials Today: Proceedings, vol. 4, iss. 9, pp. 9879–9882, 2017, doi: 10.1016/j.matpr.2017.06.286

[8] W.K. Chan, *Detection of cavitation erosion in centrifugal pumps*, International Journal of Heat and Fluid Flow, vol. 9, iss. 1, pp. 74-77, 1988, doi: 10.1016/0142-727X(88)90033-1

[9] B.K. Gandhi, S.N. Singh, V. Seshadri, *Study of the parametric dependence of erosion wear for the parallel flow of solid–liquid mixtures*, Tribology International, vol. 32, iss. 5, pp. 275–282, 1999, doi: 10.1016/s0301-679x(99)00047-x

[10] A. Rawat, S.N. Singh, V. Seshadri, *Erosion wear studies on high concentration fly ash slurries*, Wear, vol. 378–379, pp. 114-125, 2017, doi: 10.1016/j.wear.2017.02.039

[11] Y. Zhong, K. Minemura, *Measurement of erosion due to particle impingement and numerical prediction of wear in pump casing*, Wear, vol. 199, iss. 1, pp. 36-44, 1996, doi: 10.1016/0043-1648(96)06974-8

[12] K.V. Pagalthivarthi, P.K. Gupta, V. Tyagi, M.R. Ravi, *CFD Predictions of Dense Slurry Flow in Centrifugal Pump Casings*, International Journal of Mechanical and Mechatronics Engineering, vol. 5, no. 3, pp. 538-550, 2011.

[13] D.R. Kaushal, T. Thinglas, Y. Tomita, S. Kuchii, H. Tsukamoto, *CFD modeling for pipeline flow of fine particles at high concentration*, International Journal of Multiphase Flow, vol. 43, pp. 85–100, 2012, doi: 10.1016/j.ijmultiphaseflow.2012.03.005

[14] D.H. Mesa, A. Toro, A. Sinatora, A.P. Tschiptschin, *The effect of testing temperature on corrosion–erosion resistance of martensitic stainless steels*, Wear, vol. 255, iss. 1-6, pp. 139–145, 2003, doi: 10.1016/S0043- 1648(03)00096-6

[15] S. Kumar, *Evalution of erosion wear of cetrifugal pump using cfd*, International Journal of Advance Research in Science and Engineering, vol. 6, iss. 12, pp. 1374-1381, 2017.

[16] Y. Xiao, B. Guo, S.-H. Ahn, Y. Luo, Z. Wang, G. Shi, Y. Li, *Slurry Flow and Erosion Prediction in a Centrifugal Pump after Long-Term Operation*, Energies, vol. 12, iss. 8, pp. 1-17, 2019, doi: 10.3390/en12081523

[17] J. Kumar, G. Tiwari, A. Rawat, V.K. Patel, *Effect of Swirl Vanes Angle on Erosion Behavior of AISI 316 Pipe Bend*, Materials Today: Proceedings, In Press, 2020, doi: 10.1016/j.matpr.2020.01.026

[18] Y.K. Baghel, J. Kumar, B. Kishor, A. Rawat, V.K. Patel, *Effect of Hot Forging on the Slurry Erosion Wear of AISI 316 and AISI 410 Steel*, Materials Today: Proceedings, In Press, 2020, doi: 10.1016/j.matpr.2020.02.366

[19] A. Tudor, R. Nehriu, I. Radu, V. Dumitru, *A Wear study case of ceramic ball seat valve*, Tribology in Industry, vol. 25, no. 3&4, pp. 83-88, 2003.

[20] D. Kekes, P. Psyllaki, M. Vardavoulias, *Wear Micro-Mechanisms of Composite WC-Co/Cr-NiCrFeBSiC Coatings. Part I: Dry Sliding*, Tribology in Industry, vol. 36, no. 4, pp. 361-374, 2014.

[21] D. Kekes, P. Psyllaki, M. Vardavoulias, G. Vekinis, *Wear Micro-Mechanisms of Composite WC-Co/Cr-NiCrFeBSiC Coatings. Part II: Cavitation Erosion*, Tribology in Industry, vol. 36, no. 4, pp. 375-383, 2014.

[22] G. Tiwari, J. Kumar, V. Prasad, V.K. Patel, *Derivation of cavitation characteristics of a 3mw prototype francis turbine through numerical hydrodynamic analysis*, Materials Today: Proceedings, In Press, 2020, doi: 10.1016/j.matpr.2020.02.297

[23] A.R. Al-Obaidi, *Investigation of effect of pump rotational speed on performance and detection of cavitation within a centrifugal pump using vibration analysis,* Heliyon, vol. 5, iss. 6, pp. 1-19, 2019, doi: 10.1016/j.heliyon.2019.e01910

[24] A.R. Al-Obaidi, *Experimental Investigation of the Effect of Suction Valve Opening on the Performance and Detection of cavitation in the Centrifugal Pump Based on Acoustic Analysis Technique,* Archives of Acoustics, vol. 44, no. 1, pp. 59–69, 2019, doi: 10.24425/aoa.2019.126352

[25] A.R. Al-Obaidi, *Monitoring the Performance of Centrifugal Pump under Single-Phase and Cavitation Condition: A CFD Analysis of the*

Number of Impeller Blades, Journal of Applied Fluid Mechanics, vol. 12, no. 2, pp. 445-459, 2019, doi: 10.29252/jafm.12.02.29303

[26] A.R. Al-Obaidi, *Effects of Different Turbulence Models on Three-Dimensional Unsteady Cavitating Flows in the Centrifugal Pump and Performance Prediction,* International Journal of Nonlinear Sciences and Numerical Simulation, vol. 20, iss. 3-4, pp. 487–509, 2019, doi: 10.1515/ijnsns-2018-0336

[27] M.A. Rayan, M. Shawky, *Evaluation of wear in a centrifugal slurry pump,* Proceedings of the Institution of Mechanical Engineers, Part A: Journal of Power Engineering, vol. 203, iss. 1, pp. 19-23**,** 1989, doi: 10.1243/PIME_PROC_1989_203_003_02

[28] Z. Shen, W. Chu, X. Li, W. Dong, *Sediment erosion in the impeller of a double-suction centrifugal pump – A case study of the Jingtai Yellow River Irrigation Project, China,* Wear, vol. 422–423, pp. 269–279, 2019, doi: 10.1016/j.wear.2019.01.088

[29] Z. Wang, Z. Qian, *Effects of concentration and size of silt particles on the performance of a double-suction centrifugal pump*, Energy, vol. 123, pp. 36-46, 2017, doi: 10.1016/j.energy.2017.01.142

[30] K.A. Kazim, B. Maiti, P. Chand, *A correlation to predict the performance characteristics of centrifugal pumps handling slurries*, Proceedings of the Institution of Mechanical Engineers, Part A: Journal of Power Engineering, vol. 211 iss. 2, pp. 147-157, 1997, doi: 10.1243/0957650971537060

[31] J.F. Gulich, *Effect of Reynolds Number and Surface Roughness on the Efficiency of Centrifugal Pumps,* Journal of Fluids Engineering, vol. 125, iss. 4, pp. 670-679, 2003, doi: 10.1115/1.1593711

[32] V. Batalovic, *Erosive Wear Model of Slurry Pump Impeller,* Journal of Tribology, vol. 132, iss. 2, p. 5, 2010, doi: 10.1115/1.4001167

[33] Y.I. Oka, T. Yoshida, *Practical estimation of erosion damage caused by solid particle impact Part 2: Mechanical properties of materials directly associated with erosion damage*, Wear, vol. 259, iss. 1-6, pp. 102–109, 2005a, doi: 10.1016/j.wear.2005.01.040

[34] Y.I. Oka, K. Okamura, T. Yoshida, *Practical estimation of erosion damage caused by solid particle impact Part 1: Effects of impact parameters on a predictive equation*, Wear, vol. 259, iss. 1-6, pp. 95–101, 2005, doi: 10.1016/j.wear.2005.01.039

[35] R. Gupta, S.N. Singh, V. Sehadri, *Prediction of uneven wear in a slurry pipeline on the basis of measurements in a pot tester*, Wear, vol. 184, iss. 2, pp. 169-178, 1995, doi: 10.1016/0043-1648(94)06566-7

Nomenclature

C_w	Concentration by weight
$E(\alpha)$	Erosion rate (kg/m^2-s^{-1})
F_1& F_2	Blending function
H_v	Hardness of solid particle
S_m	Mass addition from a source term
CS	Carbon steel
SS	Stainless steel
α	Particle impact angle,
v	Impact velocity (m/s),
μ_t	Turbulent viscosity,
Γ_k, Γ_ω	Effective diffusivities,
τ_r	Particle relaxation time